30min-Ahead Gridded Solar Irradiance Forecasting using Satellite Data

Todd Taomae[1], Lipyeow Lim[1], Duane Stevens[1], and Dora Nakafuji[2]

[1] University of Hawai'i at Mānoa, Honolulu, HI, USA.
[2] Hawaiian Electric Company, Honolulu, HI, USA.

Abstract. Solar irradiance forecasting is critical to balancing solar energy production and energy consumption in the electric grid; however, solar irradiance forecasting is dependent on meteorological conditions and, in particular, cloud cover, which are captured in satellite imagery. In this paper we present a method for short-term solar irradiance forecasting using gridded global horizontal irradiance (GHI) data estimated from satellite images. We use this data to first create a simple linear regression model with a single predictor variable. We then discuss various methods to extend and improve the model. We found that adding predictor variables and partitioning the data to create multiple models both reduced prediction errors under certain circumstances. However, both these techniques were outperformed by applying a data transformation before training the linear regression model.

1 Introduction

One of the key problems faced by electric grid operators when integrating solar energy sources is the uncertainty in the production of solar energy. Most electric grid have very limited energy buffering capabilities, hence grid operators have to carefully match energy production to energy consumption. Energy consumption, also known as load, is relatively well understood to follow certain diurnal and seasonal patterns. In contrast to traditional oil-based energy generation, solar energy production is less well characterized and is dependent on atmospheric conditions, in particular, cloud cover.

In this paper, we study the problem of short term solar irradiance prediction using time series satellite imagery data over a 72 kilometer by 58 kilometer region covering the island of O'ahu in the state of Hawai'i. Short term is defined to be 30 to 90 minutes lead time. The satellite imagery data is collected via geostationary satellites and converted to gridded Global Horizontal Irradiance (GHI) data using the Perez method [20] (we will still call these gridded GHI data "images"). GHI is the total solar radiation received by a surface horizontal to the ground and is measured in watts per square meter (W/m^2). The computational problem can be described as: given a time series of GHI images, predict or forecast the next GHI image. In this paper, we investigate linear regression-based models for this computational prediction task where each pixel in the predicted images is dependent on surrounding pixels in the images of several previous time steps.

This model is inspired by the atmospheric phenomenon known as persistence which essentially captures the locality of weather phenomena both spatially and temporally. We further investigate how different ways of partitioning the data and transforming the data can improve the performance of the prediction.

We tested our models on two years worth of satellite imagery data (2014-2014) using 2013's data as training and 2014's data as a testing data set. Our experiments show that the linear regression models perform surprisingly well. The best prediction error in terms of mean absolute error is 80.21 W/m^2 - the maximum solar irradiance during the sunniest part of the day is approximately 1600 W/m^2.

The rest of this paper is organized as follows. Section 2 describes related work. Section 3 describes satellite imagery data set used in this study. Section 4 details the various linear regression-based models used for predicting the GHI images. Section 5 presents the results of our investigation. Section 6 concludes the paper.

2 Related Work

There is a large body of work which has investigated solar irradiance forecasting with forecast horizons ranging from 5 minutes to 15 days. These methods can generally be broadly grouped into one of three different categories [6]. The first category consists of statistical models which are based on historical solar irradiance data. Another set of methods are based around cloud motion determined either from satellite images or from ground-based sky images. The last type of solar forecasting is based on a technique known as numerical weather prediction which uses observed weather variables as input into computer models which try to forecast the future state of the weather. A fourth category of hybrid models also exists.

Each of these categories of methods tend to perform better for different timescales. Statistical models and cloud motion based methods are typically used for forecasts up to 6 hours, while numerical weather prediction models perform better beyond the 6 hour range. These methods also operate at different spatial resolution. While numerical weather prediction can provide more accurate forecasts at larger timescales, it comes at the cost of much lower spatial resolution. Rather than operating at resolutions of 1 kilometer or less, numerical weather prediction is limited to resolutions on the order of 10 to 100 kilometers.

Statistical models can be further divided into linear and non-linear models. The simplest linear model is known as the persistence model or naïve predictor model and simply assumes that the solar irradiance at time t is equal to the irradiance at $t-n$. This method is sometimes used as a baseline for comparison to other methods. Other examples of linear models are autoregressive moving average (ARMA), autoregressive integrated moving average (ARIMA) [1, 13], and coupled autoregressive and dymical system (CARDS) [14]. Non-linear methods include artificial neural networks [9, 12, 17] and wavelet neural networks [3, 19].

Besides daily and annual irradiance patterns, which are deterministic based on the rotation and revolution of the earth, cloud cover is the main influence on solar irradiance at the surface. This is the basis for cloud motion based methods. These methods use either satellite images [10, 11, 16] or ground-based sky images [5] to extrapolate cloud motion based on recordings at previous time steps. Ground-based images can provide a much higher temporal and spatial resolution, but at the cost of much lower coverage.

Numerical weather prediction models attempt to model the state and evolution of the atmosphere using partial differential equations based on the laws of physics. Examples of numerical weather prediction models include the Global Forecast System (GFS) [8], the Integrated Forecast System (IFS) [18], and the Weather Research and Forecasting (WRF) Model [7].

The GFS and IFS models are both global models while WRF is a higher resolution, *mesoscale* model. IFS is also an example of an ensemble model which runs multiple simulations using slightly different initial conditions. This is used to help account for the uncertainty of initial observations and the chaotic nature and sensitivity to initial conditions of weather systems.

Hybrid models are used in an attempt to overcome limitations of methods using individual models. Examples of hybrid models include combining ARMA or ARIMA with neural networks [15, 21], combining neural networks and fuzzy logic [3], and combining neural networks with wavelet analysis [2, 4]

3 Satellite-derived Global Horizontal Irradiance Data Set

The data set used in our experiments consists of Global Horizontal Irradiance (GHI) data estimated from satellite images using the Perez method [20] for a region surrounding Hawaii for the years 2013 and 2014. The data was provided by AWS Truepower.

The data set contains GHI information for a grid of 1,120 by 1,040 points at a 2 kilometer resolution, centered over Hawaii. However, for this paper we will focus on a 36 by 29 grid over Oahu, which is shown in Figure 1.

While the data set contains data for most of the day, we will focus on only the subset between 8AM and 5PM Hawaii Standard Time (HST). The reason for this choice is that we are guaranteed to have non-zero GHI throughout the entire year during this time interval. Most of the data is provided at 15 minute intervals; however, there are some gaps of 30 minute intervals. Fig. 3 shows the times at which GHI data is available, within the window in which we are interested. The rows identify the hour in HST and the columns identify the minute within the hour. There is also some data missing throughout both years resulting occasional gaps greater than 30 minutes and up to several hours.

We will use the following notation to represent the GHI at the grid coordinate (x, y) at time t.

$$S(x, y, t)$$

While specific values are not of interest to us, this notation allows us to easily discuss relative times and location. For example, $S(x + 1, y - 1, t - 60)$ refers to

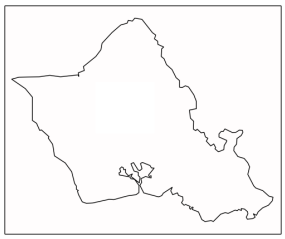

Fig. 1: GHI map

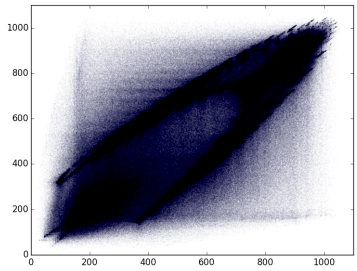

Fig. 2: $S(x, y, t)$ vs. $S(x, y, t - 60)$

	00	15	30	45
08	x		x	x
09	x	x	x	x
10	x	x		x
11	x		x	x
12	x	x	x	x
13	x	x	x	x
14	x		x	
15	x	x	x	x
16	x	x	x	x

Fig. 3: Times available for GHI data

the GHI at the grid point one unit to the east and one unit to the south of (x, y) at the time 60 minutes before t.

4 1-Hour Ahead Solar Forecasting via Linear Regression

In this section we describe a method for making approximately 1-hour ahead predictions of the solar irradiance at a given location. We will call the time for which we wish to predict the GHI, time t. We will use information available to us at time $t - n$, where n is the number of minutes prior to t at which we are making the prediction. Intuitively, one might expect that the solar irradiance at $t - n$ at the same location would be a good predictor for our target. This is the basis on which we build linear regression models for forecasting GHI.

Linear regression is a method for modeling the relationship between a dependent variable and one or more predictor variables. In our case, the dependent variable is $S(x, y, t)$ and, in the simplest example, the predictor variable is $S(x, y, t-n)$. In this example with a single predictor variable, we wish to create a model as shown in Eqn. 1 with constants c_1 and c_0 that will minimize the sum of the squared residuals, by way of ordinary least squares. The residual is the difference between the observed $S(x, y, t)$ and the value estimated by the linear regression model. This model will be based on all possible $S(x, y, t)$ and $S(x, y, t - n)$ for the region surrounding Oahu (shown in Figure 1) during 2013.

$$S(x, y, t) = c_1 S(x, y, t - n) + c_0 \tag{1}$$

This can also described visually. Figure 2 is a scatter plot of the GHI for a given point at time t versus the GHI at that same point at $t-60$ for a portion of the data set. The residual is the vertical distance between a point and the line given by Eqn. 1. So the goal of a linear regression is to choose c_1 and c_0 such that we minimize the sum of the squared vertical distances.

The model described above relies on a few assumptions. We are assuming that the GHI patterns are the same for all points on the grid, for all times of

the day, and for all days of the year. However, this is obviously not true. For example, during the mornings GHI will generally trend upward while in the afternoons it will trend downward. While these assumptions allowed us to make a simple model, we will show later that it results in relatively poor performance. Throughout the remainder of this section, we will discuss various techniques to potentially increase the accuracy of our model. These techniques all work independently of each other and can be used individually or in combination with each other. First we will discuss including additional predictor variables, followed by partitioning the data and creating separate models for each partition of data, and lastly we will discuss a technique where we transform the data and use the transformed data to create the models.

4.1 Adding Predictor Variables

When using the simple model described above, there may be important information that is not captured by using only a single predictor variable. We can add predictor variables by either expanding temporally or spatially.

If we expand temporally, we would include more past data. Instead of using only data at $t - n$, we can, for example, use $[t - n_0, t - n_1, \ldots, t - n_m]$. Since we are including additional predictor variable, obviously our original model will no longer work. Instead, we will have a model that looks like Eqn. 2 which uses data from k past times and will have constants c_k and c_0.

$$S(x, y, t) = \left(\sum_{k=1}^{m} c_k S(x, y, t - n_k) \right) + c_0 \tag{2}$$

If we expand spatially, we include data from neighboring grid points. We define r as the "radius" of the surrounding region, which will be centered on (x, y). The model is now defined by Eqn. 3. Constants are not indexed by i and j.

$$S(x, y, t) = \left(\sum_{i=-r}^{r} \sum_{j=-r}^{r} c_{i,j} S(x + i, y + j, t - n) \right) + c_0 \tag{3}$$

We can also combine both of these techniques and expand both temporally and spatially. The resulting model is given by Eqn. 4. We now index constants by i, j, and k.

$$S(x, y, t) = \left(\sum_{i=-r}^{r} \sum_{j=-r}^{r} \sum_{k=1}^{m} c_{i,j,k} S(x + i, y + j, t - n_k) \right) + c_0 \tag{4}$$

Figure 4 shows an example which uses both of these techniques. The red square in Figure 4c represents $S(x, y, t)$ and the red boxes in Figures 4b and 4a are our predictor variables.

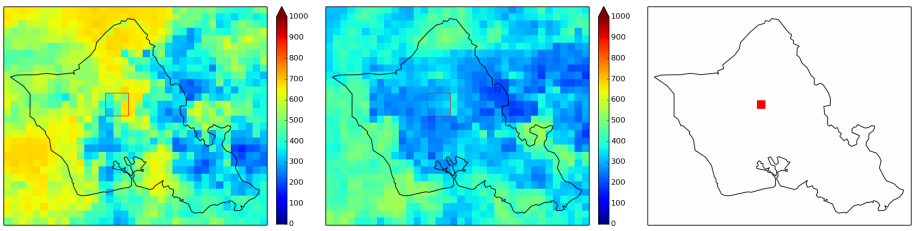

(a) $t - n_1$: Predictors. (b) $t - n_0$: Predictors. (c) t: Target.

Fig. 4: Predictors and Target

4.2 Partitioning Data

In the original model, we made several assumptions which led to a single model for all data. However, it is unlikely that GHI patterns will be the same for all points on the grid, for all times of the day, and for all days of the year. In order to account for such differences, we can partition the data based on these differences and create separate models for each partition. This partitioning can be either temporal or spatial.

Temporal Partitioning There are two main ways that we might partition the data temporally. We can partition on either a daily or yearly scale. On a daily scale, we might, for example, want to create a different model for each hour of the day, while on a yearly scale, we might create a different model for each month of the year. It is also possible to combine both of these which would leave us with a different model for each hour of each month.

While partitioning the data at this granularity could potentially provide more accurate models, it also means that we will have less data to train each model and we will have many more models. If we were to combine both hourly and monthly partitioning, we would end up with 108 different models, each with approximately 108 times less data (9 hours between 8AM and 5PM; 12 months in a year).

Rather than partitioning by each hour, a more reasonable approach might be to simply partition the data into morning and afternoon. This also has some intuitive justification since there is a clear distinction in general GHI patterns in the morning and afternoon. In the morning, we expect the GHI to generally be increasing, while in the afternoon it will tend to decrease. The hope is that these patterns can be more accurately captured by the linear regression models if they separated.

On the yearly scale, it is less obvious how to partition the data. Seasonal partitioning might be a good candidate. However, since the seasonal patterns are not as distinct in Hawaii as many other places we will focus on a bi-annual partition. We will refer to the combination of winter and spring as “winter” and the combination of summer and autumn as “summer.” While using equinoxes

and solstices as the seasonal boundaries might provide slightly more accurate models, for convenience, we will divide seasons on monthly boundaries. Each season will consist of three months, starting with winter consisting of December, January, and February and the rest of the seasons following in three month chunks.

Spatial & Elevation Partitioning In addition to partitioning temporally, we can also perform spatial partitioning. On a global scale, it makes sense that, for example, the GHI patterns in Hawaii will be very different from those in Alaska. However, since we are only considering Oahu, it is less obvious how we might partition the data.

One way that we might partition the data is by land and ocean. This particularly makes sense for our application since there are obviously no rooftop solar panels or solar farms in the ocean. Another, perhaps less obvious, way to partition the data is by elevation. There are two main motivations behind partitioning by elevation. First, more of the population lives at lower elevation. Therefore, there will likely be more rooftop solar panels in that region. The second motivation has a meteorological basis; due to warm air rising along the mountains, cloud formation is more likely at higher elevations as the air cools and condenses.

We obtained elevation data from the Google Maps Elevation API. From this we can easily partition each grid point by elevation, but we can also use this to approximate which grid points are on the land or ocean. We consider any point with an elevation of 0 meters or less to be part of the ocean and any point with greater than 0 meters elevation to be part of the land.

4.3 Data Transformation

In this section we describe a method for processing the GHI data which provides an alternative method to account for differences in time of day and location that does not reduce the amount of data that we have to create the model as was the case with partitioning. Let $\hat{S}(x, y, t)$ denote the transformed value. After we apply the transformation, the data can be used as before. For example, Eqn. 5 defines the linear regression model equivalent to the one give by Eqn. 1.

$$\hat{S}(x, y, t) = c_1 \hat{S}(x, y, t - n) + c_0 \tag{5}$$

Our transformation will be based on the deviation from some average value. Consider the following scenario. Suppose that the GHI at some location is 500 $\mathrm{W/m^2}$. If this is in the afternoon, then this might be a normal value for that time of day, so we might expect that it will follow typical patterns. However, if this is in the middle of the day, then it might be lower than we expect, so we probably would not expect it to follow typical patterns. This is the motivation behind this model. We also take into account the fact that the typical value at a given time of day might vary from one location to the next.

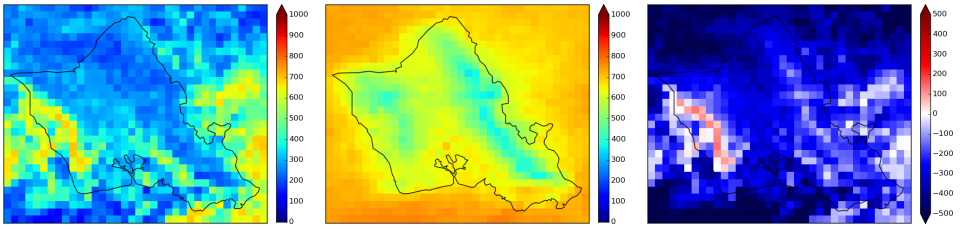

(a) Actual data for 2013-01-01T12:00HST. (b) Average for 12:00HST. (c) Deviation from average for 2013-01-01T12:00HST.

Fig. 5: Process for computing deviation

Following the reasoning from the example above, our averaging should take into account both temporal and spatial information. This is accomplished by computing the average for each grid point at each time of day. Let $\bar{S}(x, y, hh{:}mm)$ represent the average GHI for a given grid point at a time of day specified by $hh{:}mm$.

The data transformation simply subtracts the corresponding average value from the actual average. For example,

$$\hat{S}(x, y, \text{2013-01-01T12:00}) = S(x, y, \text{2013-01-01T12:00}) - \bar{S}(x, y, \text{12:00}).$$

Figure 5 shows the process visually. Figure 5a shows the data for one specific day at noon and Figure 5b shows the average that was computed from all the data at noon. Lastly, Figure 5c shows the deviation from the average for one specific day at noon, obtained by subtracting the values in 5b from 5a. This is data that will be used for creating the linear regression model.

5 Results

Due do the number of combinations that are possible as well as the number of parameters that can be adjusted, it would be unreasonable to test all possible models. Also, due to our limited data set, it would not make sense to try all possible combinations to find one that is the best as it would likely be specific to our data set. Rather, it is more important to find which techniques seem to reduce errors in general.

This section will describe the performance of a number of different models. Each model is created using 2013 data only and predictions are made for 2014. It is important to note that when applying the data transformation, the average is based only on 2013 and when computing the deviation from the average, even for 2014 data, we will use the 2013 average. The performance will be measured by mean absolute error (MAE). In other words, the average of the absolute difference between our prediction and the actual irradiance. In the tables listing the results, we will also report the standard deviation in parentheses.

5.1 Accuracy vs. Spatial and Temporal Resolution

Tables 1, and 2 show the performance of our method as we increase the amount of spatial or temporal data used. The labels on the top and left describe how many predictor variables are used in each model. The spatial data is labeled as $n \times n$ which describes the size of the surrounding region that we will use. The temporal data is labeled as a list of times used, relative to the target time. "(DT)" indicates that our data transformation was applied to that particular model.

From Table 1 we can see that the error of our model decreases consistently up to a 13×13 region. However, the improvement is largest when moving from 1×1 to 3×3 and anything beyond 5×5 seems to have very minimal impact. We have not tested using regions larger than 13×13 so it is not clear what will happen beyond that point. However, we suspect that at some point it will include too much information from too far away and performance will degrade.

Table 1 also shows the impact of increasing from 30 to 60-minute predictions. The result is not very surprising. As we try to forecast farther into the future, the error increases.

Table 2 also shows the impact of including more temporal data. What is interesting here is that when we do not apply the data transformation, using up to 90 minutes of temporal data does not have much impact, but using up to 120 minutes of temporal data reduces the prediction error by a significant margin. In contrast, if we do apply the data transformation, adding temporal data does not help and in fact increases error.

Table 2 shows the effect of including both temporal and spatial data. This table suggests that the two factors work mostly independently of each other. Adding spatial data helps in all cases, as it did in Table 1, and adding temporal data helps in the same way as it did in Table 2. Specifically, if the data transformation was not applied, then the additional temporal data seems to help.

5.2 Accuracy using Temporal & Elevation Partitioning

The results of applying temporal and elevation partitioning are shown in Tables 3 and 4. These results are based on a model which uses a single predictor variable for 60-minute forecasts. Table 3 shows the performance of various combinations of daily and yearly partitioning and Table 4 shows the performance for various elevation partitions. In addition to the mean absolute error and standard deviation, we also report — in square brackets and italics — the mean absolute error of the equivalent non-partitioned model, for the partition in question. In particular, we use the results from the non-partitioned, non-transformed, single predictor variable model and rather than looking at the error across all predictions, we look at the error specifically for only morning hours, or only afternoon hours, etc. This will allow us to see if the performance is truly improving.

We can see from Table 3 that temporal partitioning is useful in all cases except for the "summer" partition. We can also see that partitioning by morning

	[t-30]	[t-30] (DT)	[t-60]	[t-60] (DT)
1×1	109.16 (140.89)	89.83 (127.52)	149.66 (178.17)	109.18 (146.64)
3×3	103.15 (133.08)	83.15 (119.87)	146.11 (173.45)	103.55 (140.32)
5×5	101.96 (131.35)	81.65 (117.89)	145.38 (172.36)	101.99 (138.34)
7×7	101.39 (130.57)	80.91 (116.89)	145.00 (171.82)	101.07 (137.20)
9×9	101.13 (130.20)	80.53 (116.36)	144.82 (171.54)	100.90 (136.48)
11×11	101.01 (130.03)	80.33 (116.06)	144.72 (171.40)	100.08 (135.98)
13×13	100.95 (129.93)	80.21 (115.90)	144.67 (171.31)	99.78 (135.64)

Table 1: MAE with increasing spatial resolution. Standard deviation in parenthesis.

	1×1	1×1 (DT)	3×3	3×3 (DT)
[t-60]	149.66 (178.17)	109.18 (146.64)	146.11 (173.45)	103.55 (140.32)
[t-60, t-90]	150.33 (180.29)	109.93 (146.96)	141.27 (172.41)	105.69 (142.49)
[t-60, t-75, t-90]	149.05 (180.93)	110.15 (147.89)	140.50 (173.17)	106.45 (143.93)
[t-60, t-90, t-120]	145.70 (177.52)	113.16 (150.09)	134.95 (167.95)	108.82 (145.81)
[t-60, t-75, t-90, t-105, t-120]	136.94 (172.04)	118.32 (156.83)	130.94 (166.13)	114.53 (153.03)

Table 2: MAE with increasing spatial resolution and temporal window.

and afternoon reduces errors much more than partitioning by seasons. This could be due to the fact that seasonal differences are not very significant in Hawaii.

Table 4 shows us that spatial partitioning is not very useful for our data set. While, in most cases, the partitioning does improve the error relative to the average error of the original model, when we compare it to the error for only that partition (the number in square brackets), the improvement is much less significant and in fact often performs slightly worse. The one exception is when elevation is greater than 500 meters. However, that only accounts for less than 10% of the total land and likely an even smaller portion of the population and rooftop solar panels.

Table 5 contains the results of applying temporal partitioning as well as data transformation. Again we see that the "summer" partition performs worse while the others perform better. However, the improvements are much less significant than applying those seen in Table 3. This is likely due to the fact that the data transformation already captures the same patterns that temporal partitioning tries to account for.

6 Conclusion

In this paper we discussed a method for short-term gridded solar irradiance forecasting using linear regression as well as several techniques for improving the linear regression model. We found that adding predictor variables was useful in reducing errors. In particular including additional spatial data improved predictions in all cases that we tested, while adding temporal data only improved

	Full Day	Morning	Afternoon
Full Year	149.66 (178.17)	109.65 (141.52) *[144.17]*	131.33 (163.59) *[152.53]*
"Winter"	144.38 (172.74) *[145.06]*	106.56 (138.74) *[134.36]*	127.13 (158.05) *[150.55]*
"Summer"	155.31 (183.12) *[153.40]*	112.64 (143.15) *[154.05]*	136.08 (169.39) *[154.58]*

Table 3: MAE with temporal and seasonal partitioning. Standard deviation in parenthesis and MAE of non-partitioned baseline in square brackets.

"Ocean" (elevation $\leq$ 0m)	152.31 (180.76) *[152.78]*
"Land" (elevation $>$ 0m)	144.37 (172.98) *[144.75]*
0m $<$ elevation $\leq$ 50m	146.95 (174.96) *[145.81]*
50m $<$ elevation $\leq$ 100m	146.19 (174.15) *[145.65]*
100m $<$ elevation $\leq$ 150m	146.68 (175.56) *[146.78]*
150m $<$ elevation $\leq$ 200m	147.53 (176.12) *[147.01]*
elevation $>$ 200m	140.90 (170.34) *[143.32]*
elevation $>$ 500m	129.06 (159.73) *[137.28]*

Table 4: MAE with elevation partitioning.

	Full Day	Morning	Afternoon
Full Year	109.18 (146.64)	104.31 (140.41) *[110.90]*	101.16 (137.18) *[108.27]*
"Winter"	107.14 (145.49) *[108.74]*	101.10 (137.32) *[109.91]*	100.62 (137.57) *[108.14]*
"Summer"	111.58 (147.40) *[109.62]*	107.80 (142.51) *[111.91]*	101.95 (138.02) *[108.41]*

Table 5: MAE with temporal, seasonal partitioning & data transformation.

predictions under certain circumstances. We used regions up to 13×13 grid points, but the rate of improvement was greatly reduced beyond a 5×5 region. Partitioning the data and creating separate models for each partition was also helpful in certain cases. Spatial partitioning turned out not to be very helpful except at high elevations which accounts for only a small portion of Oahu. Temporal partition was more useful with dividing the data into morning and afternoon partitions reducing the errors the most. All of the above methods were out-performed by first applying a data transformation which takes into account different patterns based on the time of day and location. In addition, this can be further improved by including additional spatial data.

References

1. Brinkworth, B.: Autocorrelation and stochastic modelling of insolation sequences. Solar Energy 19(4), 343–347 (1977)
2. Cao, J., Cao, S.: Study of forecasting solar irradiance using neural networks with preprocessing sample data by wavelet analysis. Energy 31(15), 3435–3445 (2006)
3. Cao, J., Lin, X.: Application of the diagonal recurrent wavelet neural network to solar irradiation forecast assisted with fuzzy technique. Engineering Applications of Artificial Intelligence 21(8), 1255–1263 (2008)
4. Cao, S., Cao, J.: Forecast of solar irradiance using recurrent neural networks combined with wavelet analysis. Applied Thermal Engineering 25(2), 161–172 (2005)

5. Chow, C.W., Urquhart, B., Lave, M., Dominguez, A., Kleissl, J., Shields, J., Washom, B.: Intra-hour forecasting with a total sky imager at the UC San Diego solar energy testbed. Solar Energy 85(11), 2881–2893 (2011)
6. Diagne, M., David, M., Lauret, P., Boland, J., Schmutz, N.: Review of solar irradiance forecasting methods and a proposition for small-scale insular grids. Renewable and Sustainable Energy Reviews 27, 65–76 (2013)
7. Dudhia, J., Gill, D., Henderson, T., Klemp, J., Skamarock, W., Wang, W.: The weather research and forecast model: software architecture and performance. In: Proceedings of the Eleventh ECMWF Workshop on the Use of High Performance Computing in Meteorology. pp. 156–168. World Scientific (2005)
8. for Environmental Information, N.C.: Global forecast system (gfs), http://www.ncdc.noaa.gov/data-access/model-data/model-datasets/global-forcast-system-gfs
9. Guarnieri, R., Martins, F., Pereira, E., Chou, S.C.: Solar radiation forecast using artificial neural networks. National Institute for Space Research pp. 1–34 (2008)
10. Hammer, A., Heinemann, D., Lorenz, E., Lückehe, B.: Short-term forecasting of solar radiation: a statistical approach using satellite data. Solar Energy 67(1), 139–150 (1999)
11. Heinemann, D., Lorenz, E., Girodo, M.: Forecasting of solar radiation. Solar energy resource management for electricity generation from local level to global scale. Nova Science Publishers, New York (2006)
12. Hocaoğlu, F.O., Gerek, Ö.N., Kurban, M.: Hourly solar radiation forecasting using optimal coefficient 2-d linear filters and feed-forward neural networks. Solar energy 82(8), 714–726 (2008)
13. Hokoi, S., Matsumoto, M., Kagawa, M.: Stochastic models of solar radiation and outdoor temperature. ASHRAE Transactions (American Society of Heating, Refrigerating and Air-Conditioning Engineers);(United States) 96(CONF-9006117–) (1990)
14. Huang, J., Korolkiewicz, M., Agrawal, M., Boland, J.: Forecasting solar radiation on an hourly time scale using a coupled autoregressive and dynamical system (cards) model. Solar Energy 87, 136–149 (2013)
15. Ji, W., Chee, K.C.: Prediction of hourly solar radiation using a novel hybrid model of arma and tdnn. Solar Energy 85(5), 808–817 (2011)
16. Lorenz, E., Hammer, A., Heinemann, D.: Short term forecasting of solar radiation based on satellite data. In: EUROSUN2004 (ISES Europe Solar Congress). pp. 841–848 (2004)
17. Martins, F.R., Pereira, E.B., Guarnieri, R.A.: Solar radiation forecast using artificial neural networks. International Journal of Energy Science 2(6) (2012)
18. for Medium-Range Weather Forecasts, E.C.: Modeling and prediction, http://www.ecmwf.int/en/research/modelling-and-prediction
19. Mellit, A., Benghanem, M., Kalogirou, S.: An adaptive wavelet-network model for forecasting daily total solar-radiation. Applied Energy 83(7), 705–722 (2006)
20. Perez, R., Moore, K., Kmiecik, M., Chain, C., Ineichen, P., George, R., Vignola, F.: A new operational satellite-to-irradiance model–description and validation. In: Proceedings of the Solar Conference. pp. 315–322 (2002)
21. Zhang, G.P.: Time series forecasting using a hybrid arima and neural network model. Neurocomputing 50, 159–175 (2003)